Structural phase transformations and nanotwin domains in $0.93Pb(Zn_{1/3}Nb_{2/3})O_3–0.07PbTiO_3$

2008 J. Phys.: Condens. Matter 20 395229

(http://iopscience.iop.org/0953-8984/20/39/395229)

J. Phys.: Condens. Matter **20** (2008) 395229 (7pp) doi:10.1088/0953-8984/20/39/395229

Structural phase transformations and nanotwin domains in $0.93Pb(Zn_{1/3}Nb_{2/3})O_3$–$0.07PbTiO_3$

W S Chang[1], L C Lim[1], P Yang[2], F-T Wang[3], C-M Hsieh[3] and C-S Tu[3]

[1] Department of Mechanical Engineering, National University of Singapore, 10 Kent Ridge Crescent, 112960, Singapore
[2] Singapore Synchrotron Light Source, National University of Singapore, 5 Research Link, 117603, Singapore
[3] Department of Physics, Fu Jen Catholic University, Taipei 242, Taiwan, Republic of China

E-mail: weisea@nus.edu.sg (W S Chang), mpelimlc@nus.edu.sg, slsyangp@nus.edu.sg and 039611@mail.fju.edu.tw (C-S Tu)

Received 24 June 2008, in final form 18 August 2008
Published 4 September 2008
Online at stacks.iop.org/JPhysCM/20/395229

Abstract

By means of combined dielectric permittivity and thermal current density measurements and *in situ* high-resolution synchrotron x-ray diffraction study, it is shown that the unpoled and poled $0.93Pb(Zn_{1/3}Nb_{2/3})O_3$–$0.07PbTiO_3$ (PZN–7%PT) single crystals undergo a $R-(R+R_{NT}+T+T_{NT})-(T+T_{NT})-C$ transformation sequence upon zero-field heating, where R, T and C are rhombohedral, tetragonal and cubic phases, respectively. Rhombohedral (R_{NT}) and tetragonal (T_{NT}) nanotwin domains were detected in the vicinity of the R–T transformation temperature (T_{R-T}) in both the unpoled and poled states. These nanotwins are likely bridging phases which help to alleviate the internal stresses accompanying the phase transformations.

(Some figures in this article are in colour only in the electronic version)

1. Introduction

Relaxor-based ferroelectric $Pb(Zn_{1/3}Nb_{2/3})O_3$–$PbTiO_3$ (PZN–PT) and $Pb(Mg_{1/3}Nb_{2/3})O_3$–$PbTiO_3$ (PMN–PT) solid-solution single crystals have been touted as the next-generation materials for future high-performance sensors and actuators owing to their superior dielectric and electromechanical properties. Despite the extensive studies that have been carried out over the decade, the physics for the superior properties of these single crystals remains not fully answered at present. The observed superior properties, notably the high piezoelectric coefficients of $d_{33} > 2500$ pC N^{-1}, high electromechanical coupling of $k_{33} > 90\%$ and large strain of $>1.7\%$ [1, 2], have been attributed to the existence of intermediate phases, i.e. monoclinic M_A and M_B (space group Cm) and M_C (space group Pm), and orthorhombic O (space group $Amm2$) phases to facilitate the polarization rotation mechanism [3–11]. The presence of the monoclinic phases, however, is doubted by some researchers who suggested that the polarization rotation mechanism is likely to give rise to the distorted rhombohedral (R) phase which can be easily mistaken as the monoclinic phases [12, 13]. Meanwhile, the observed monoclinic phases may instead be those of coherent diffractions of rhombohedral nanotwins (R_{NT}) and tetragonal nanotwins (T_{NT}) [14, 15]. Experimental evidence of nanotwins in PMN–33%PT has been reported by transmission electron microscopy and polarized light microscopy [16], and in unpoled PZN–4.5%PT by means of a combined property measurement and high-resolution x-ray diffraction (HR-XRD) technique [17]. It should be noted that the domain structures of these exciting crystals are affected by the different processing histories of the crystals [18]. Therefore, thermal and electrical prehistories of the crystals must be taken care of before examining the domain structures and phase transformations in relaxor single crystals.

The aim of this work is to investigate the thermally induced structural transformations of both unpoled (i.e.

annealed) and annealed-and-poled PZN–7%PT single crystals by means of dielectric permittivity measurements, thermal current density measurements and HR-XRD technique. Combining bulk property characterization (i.e. dielectric permittivity and thermal current density measurements) and microstructural studies (i.e. HR-XRD) together is important in such investigations because phase transformations of these single crystals are highly affected by the polarizability of the relaxor-ferroelectric state. In this study, annealed PZN–7%PT samples of the same wafer with no prehistory of electric (E) field application were used as the starting material.

2. Experimental procedure

PZN–7%PT single crystals grown by the improved flux method [19] were supplied by Microfine Materials Technologies P/L (Singapore). The crystal was oriented by means of the Laue back-reflection method and sliced into specimens of $[100]^L \times [010]^W \times [001]^T$ in orientation. The directions are referred to as the pseudocubic (pc) coordinates. They were then diced into bar samples of $2^L \times 1^W \times 6^T$ mm^3 and $6^L \times 2^W \times 1^T$ mm^3 in dimensions. All the samples were annealed at 257 °C for 1 h prior to any experimental measurements.

For dielectric measurements, gold electrodes were deposited on the $6^L \times 2^W$ faces by dc sputtering. A variable-frequency Wayne–Kerr analyzer PMA3260A was used to obtain the real part (ε') of the dielectric permittivity. A Janis CCS-450 cold-head was used with a Lakeshore 340 controller for temperature-dependent measurements. For the unpoled sample, a 'zero-field-heating (ZFH)' process was used in which the data were taken upon heating without any E field. The heating rate used was 1.5 °C min^{-1}. For the poled sample, prior poling was performed at room temperature with a dc E field of 0.7 kV mm^{-1} along the [001] thickness direction before the samples were subjected to the ZFH process at the same heating rate. ZFH current density measurements were carried out on both the unpoled and poled samples by using a Keithley 6517A electrometer.

The HR-XRD measurements were performed at the Singapore Synchrotron Light Source (SSLS). To avoid possible surface strain effects produced by mechanical polishing, HR-XRD was taken from the fractured surface only [20, 21]. 8.048 keV photons (0.15405 nm in wavelength) were used. The incident x-ray beam had typical divergence of about 0.01°, with the best divergence being 0.006°. A series of rocking ($\Delta\omega$) scans at a range of 2θ were carried out to form the (002) reciprocal space mappings. The rocking scans were performed at the step size of 0.02° with the counting time 0.5 s for every rotating step. More experimental details can be found in [17, 22].

3. Results

3.1. Dielectric permittivity measurements

Figure 1(a) shows the real part of the ZFH dielectric permittivity (ε') of the unpoled (annealed) PZN–7%PT sample

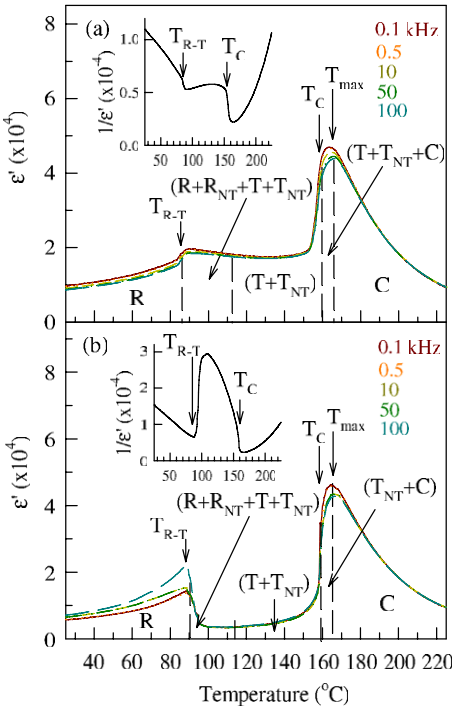

Figure 1. Temperature-dependent dielectric permittivity (ε') curves of (a) unpoled (annealed) and (b) annealed-and-poled PZN–7%PT under a ZFH process. The insets show the plot of $1/\varepsilon'$ versus temperature. Sample thickness is 1.0 mm.

measured at various frequencies (0.1–100 kHz). The ε' increased gradually with temperature initially, followed by a weak anomaly near 90 °C. This anomaly can be more readily seen in the plot of $1/\varepsilon'$ versus temperature (inset of figure 1(a)). The ε' remains relatively constant on further heating until about 160 °C. Over the temperature region of 160–165 °C, the second anomaly (and a sudden plunge in $1/\varepsilon'$) accompanied with a broad frequency-dependent maximum was observed at T_{max} (i.e. temperature at ε' maximum). This broad frequency-dependent maximum has been attributed to the dynamic relaxation processes of polar nanoclusters in the material [23].

Figure 1(b) shows the ZFH dielectric spectra after poling with $E = 0.7$ kV mm^{-1} at room temperature. Two dielectric anomalies were displayed at temperatures similar to those of the unpoled sample, being at about 90 and 165 °C, respectively. The former is characterized by a decrease in ε' at about 90 °C after a gradual increase of ε' from room temperature, while the latter is characterized by a broad frequency-dependent dielectric maximum of ε' at $T_{max} \approx 165$ °C. These anomalies can also be well observed in the $1/\varepsilon'$ versus temperature plot (inset of figure 1(b)), which shows the abrupt changes in $1/\varepsilon'$ at respective temperatures, suggesting that the two phase transformations involved are both of first order in nature.

3.2. Thermal current density measurements

The temperature-dependent current density obtained from the unpoled crystal is shown in figure 2(a). There were hardly any current signals until about 95 °C where a string of current

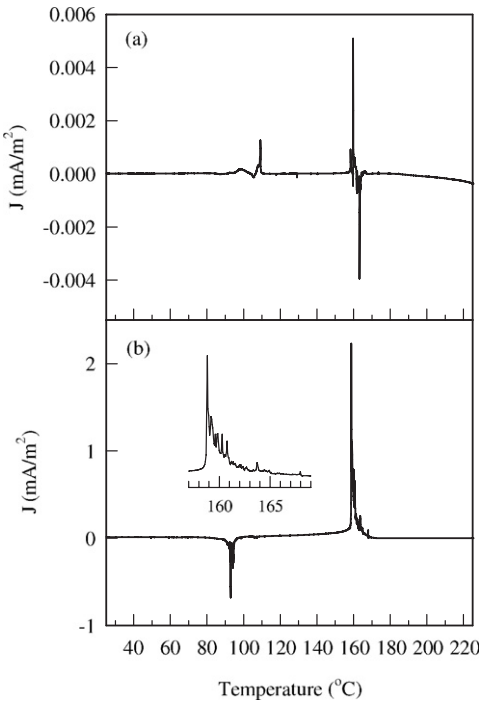

Figure 2. Thermal current density (J) of (a) unpoled (annealed) and (b) annealed-and-poled PZN–7%PT under a ZFH process. Sample thickness is 1.0 mm.

signals occurred in the region of 95–110 °C. Of these current activities, a clear current response appeared at 110 °C. There followed a region where no major current activities were detected until at about 160 °C, at which a new string of strong current signals was detected over the temperature range of 160–165 °C.

Figure 2(b) shows the current density plot of the 0.7 kV mm^{-1} poled sample. Two groups of current activities, being three orders of magnitude higher than the unpoled sample, were displayed in the temperature regions almost similar to those of the unpoled sample. The first group, being detected over the temperature region of 90–95 °C, is followed by a region where no major current activities were detected upon heating. The observed anomalous responses of the poled sample can be linked to the thermally induced depolarization [15–18]. At about 160 °C, strong current activities were again detected.

3.3. HR-XRD reciprocal space mappings

3.3.1. Unpoled (annealed) PZN–7%PT. To study the structural transformations of unpoled PZN–7%PT single crystals, HR-XRD as a function of temperature was performed on a deliberately fractured, relatively strain-free surface of a bulk sample [20, 21]. Figure 3 shows the typical (002) mappings of the unpoled sample taken over the temperature range of 25–175 °C. At 25 °C, a broad single peak with $2\theta \approx 44.64°$ lying at $\omega = 0°$ plane was detected (figure 3(a)). This broad single peak is a result of the fourfold degeneracy and high elastic compliance of the R domains. A sample showing similar diffraction mapping was pulverized into powder (of >38 μm in particle size) and standard x-ray diffraction was performed on it. The result confirmed that the phase present was the R phase, giving the refined lattice constants $a_R \approx 4.051(1)$ (or $2\theta \approx 44.70°$) and rhombohedral angle, $\alpha_R \approx 89.9725°$. The slight difference in the 2θ values between the bulk and powder samples can be attributed to the slight composition variation of the samples used. This is supported by the result of our polarized light microscopy which showed that the domains exhibited complete extinction at 25 °C when the polarizer and the analyzer pair are at the angle 45° to the [100] crystal edge, i.e. $P/A = 45°$, as shown in figure 3(i). Thus, the observed phase at room temperature is the R phase. Note from figure 3(a) that, besides the main R peak, a weak peak located at $2\theta \approx 44.90°$ and lying out of the $\omega = 0°$ plane can be detected.

With increasing temperature, the R phase remained as the stable phase with its broadness gradually reduced in both the 2θ and ω planes. Figure 3(b) gives the (002) mapping taken at 95 °C. It is interesting to note that the weak peak at $2\theta \approx 44.80°$–$44.85°$ persisted with the main R peak. We shall discuss the nature of this weak peak later.

At 100 °C (figure 3(c)), subtle changes in the diffraction mapping can be noted, i.e. new diffraction peaks at $2\theta \approx 44.40°$–$44.45°$ and $2\theta \approx 44.80°$ emerged. At 105 °C, in addition to the existing main R peak (i.e. d_4) and the weak peak (i.e. d_3 that has existed since 25 °C), five new peaks (i.e. d_1, d_2, d_5, d_6 and d_7) became evident (figure 3(d)). These peaks lie in three Bragg's positions, with peaks d_1, d_2 and d_3 lying at $2\theta \approx 44.80°$, d_4 at $2\theta \approx 44.60°$, and d_5, d_6 and d_7 at $2\theta \approx 44.46°$. Note that peaks d_2, d_4 and d_6 lie in the $\omega = 0°$ plane, while the remaining peaks lie out of the $\omega = 0°$ plane.

Upon increasing the temperature to 115 °C, six peaks were diffracted (figure 3(e)). Of the six peaks, d_1, d_2 and d_3 lie at $2\theta \approx 44.80°$ and d_4, d_5 and d_6 lie at $2\theta \approx 44.48°$. Note that peaks d_1 and d_3 at this temperature are separated by a significantly larger $\Delta\omega$ ($\approx$0.46°) values as opposed to peaks d_1 and d_3 at lower temperatures (with $\Delta\omega \approx 0.28°$). As will be explained below, the two sets of diffractions that occurred concurrently at $\approx$105 °C and $\approx$115 °C are different diffractions corresponding to those of R_{NT} and T_{NT} domains, respectively. In other words, our HR-XRD results show that ($R + R_{NT}$) and ($T + T_{NT}$) coexisted over the temperature range of 100–115 °C.

Upon heating to 155 °C (figure 3(f)), the six diffraction peaks persisted despite slight changes in their 2θ positions, from the initial value of $2\theta \approx 44.80°$ to $2\theta \approx 44.75°$ for d_1, d_2 and d_3, and from $2\theta \approx 44.45°$ to $2\theta \approx 44.53°$ for d_4, d_5 and d_6, with the off $\omega = 0°$ peaks shifting towards the $\omega = 0°$ plane (figures 3(e) and (f)). The C phase, at $2\theta \approx 44.67°$ ($\Delta\omega = 0°$), started to emerge at 160 °C (figure 3(g)) with further reduction of the diffraction intensity of the other remaining peaks. Above 165 °C, the C phase, at $2\theta \approx 44.67°$, remained as the dominant phase (figure 3(h)).

3.3.2. Poled PZN–7%PT single crystal. A similar fracturing procedure was used to prepare the poled PZN–7%PT sample for the HR-XRD study. Figure 4 shows the $(002)_{pc}$ HR-XRD mappings of the poled sample. At 25 °C, the sample revealed a broad R peak at $2\theta \approx 44.66°$ lying in the $\omega = 0°$

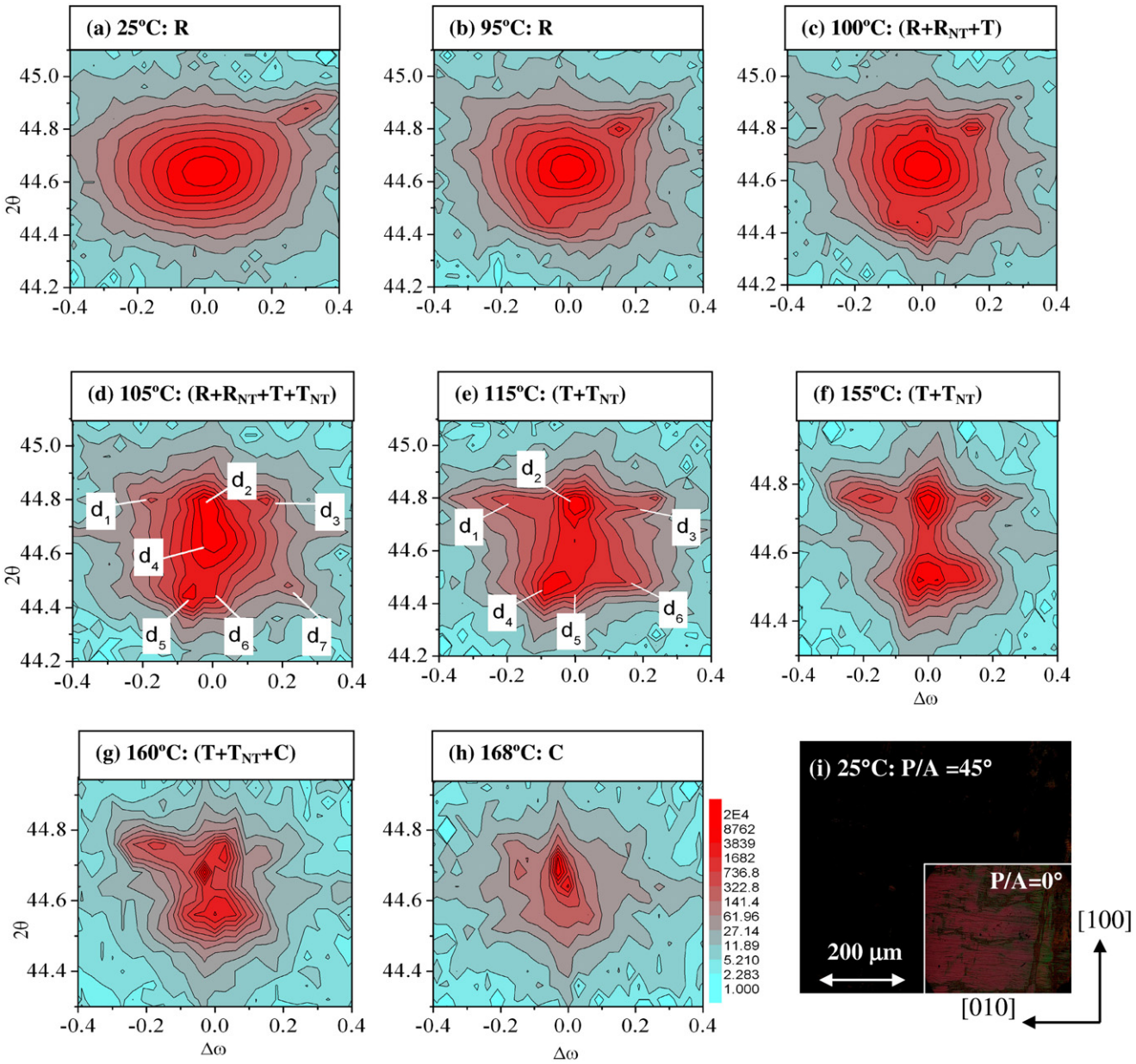

Figure 3. (a)–(h) are $(002)_{pc}$ mappings taken from the fractured surface of an unpoled (annealed) PZN–7%PT at: (a) 25 °C, (b) 95 °C, (c) 100 °C, (d) 105 °C, (e) 115 °C, (f) 155 °C, (g) 160 °C and (h) 168 °C. The intensity contours are in log scale. Figure 3(i) shows the PLM domain structures taken from a 100 μm thick unpoled PZN–7%PT sample at 25 °C.

plane (figure 4(a)). Compared with the unpoled sample, it is interesting to note that the R peak of the poled sample appeared to elongate in the 2θ plane, suggesting that a poled R crystal must be in a strained state as the result of poling-induced stresses. A similar finding has also been noted by Liu and Lynch [24]. The result shown in figure 4(a) is also consistent with our PLM result which shows that the domain matrix exhibited complete optical extinction at $P/A = 45°$ (see figure 4(i)). The R peak remained as the only diffracted peak upon heating to 100 °C ($2\theta \approx 44.63°$) (figure 4(b)).

At 110 °C (figure 4(c)), in addition to the main R peak (i.e. d_3) at $2\theta \approx 44.63°$, a new diffraction peak (i.e. d_1 at $2\theta \approx 44.84°$ with $\Delta\omega = 0°$) can be detected. This peak can be assigned to the [100] T domains, signifying the emergence of a T phase. Since d_2 peak ($2\theta \approx 44.84°$ with $\Delta\omega \neq 0$) is closely associated with the d_1 peak. This peak must thus arise from the T_{NT} domains. Diffraction peak, d_1, however, was vaguely detected. As shown in figure 4(d) at 113 °C, the R main peak gave way to R_{NT} and new diffraction peaks, marked as d_1 to d_8. As will be explained below, the d_1 to d_8 peaks correspond to the R_{NT} (d_7 and d_8), T (d_2 and d_5) and T_{NT} (d_1, d_3, d_4 and d_6) domains. The existence of R_{NT} and T_{NT} is believed to serve as a means to alleviate the internal stresses accompanying the R–T transformation.

The diffraction mappings remained relatively unchanged from 115 to 155 °C (figures 4(e) and (f)). As temperature increased further, all six diffraction peaks gradually coalesce into a single peak. Figure 4(g) shows a major diffracted

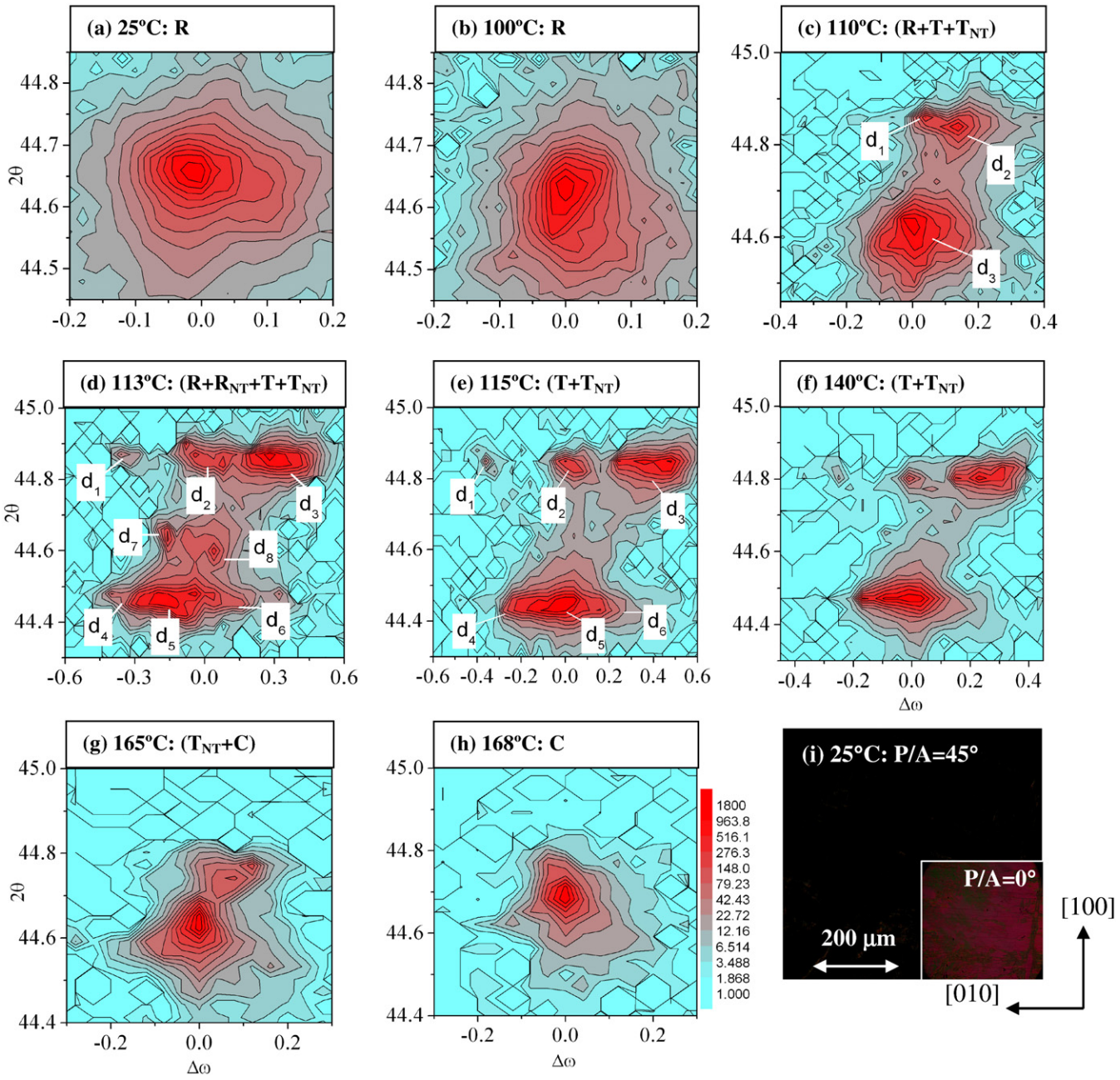

Figure 4. (a)–(h) $(002)_{pc}$ mappings taken from the fractured surface of an annealed-and-poled PZN–7%PT at: (a) 25 °C, (b) 100 °C, (c) 110 °C, (d) 113 °C, (e) 115 °C, (f) 140 °C, (g) 165 °C and (h) 168 °C. The intensity contours are in log scale. Figure 4(i) shows the PLM domain structures taken from a 100 μm thick poled PZN–7%PT sample at 25 °C.

peak at $2\theta \approx 44.64°$ together with a few obscure peaks at $2\theta \approx 44.74°$ and $2\theta \approx 44.77°$ (as the result of coalescence of the six diffraction peaks) at 165 °C. Only the major peak at $2\theta \approx 44.69°$ persisted to 168 °C, which is identified as the *C* phase (figure 4(h)).

4. Discussion

4.1. Identification of rhombohedral nanotwin diffractions

As discussed above, additional diffraction peaks other than the main *R* peak were displayed by the unpoled sample over the temperature range of 25–115 °C (figures 3(a)–(d)). These diffraction peaks may be assigned as those arising from any of the monoclinic phases or that of R_{NT}.

Table I, taken from [17], gives the various characteristics of corresponding a_{pc}, b_{pc} and c_{pc} diffractions in (002) mappings of various monoclinic phases. It shows that for M_A: $c_{pc} > a_{pc} = b_{pc}$, where a_{pc}, b_{pc} and c_{pc} are all degenerated. For M_B: $c_{pc} < a_{pc} = b_{pc}$, where a_{pc}, b_{pc} and c_{pc} are all degenerated. And for M_C: $c_{pc} > a_{pc}$ and b_{pc}, where both a_{pc} and c_{pc} are degenerated but not b_{pc}.

From table 1, the weak diffraction peaks displayed in figure 3(d) may be assigned to those of either the monoclinic

Table 1. Relationship between the monoclinic and pseudocubic axes for various monoclinic phases in the unpoled state.

Type of monoclinic	Monoclinic (mirror) plane and characteristics of a_m, b_m and c_m[a]	Relationship between monoclinic and pseudocubic axes	Characteristics of a_{pc}, b_{pc}, and c_{pc} in $(002)_{pc}$ mapping
M_A[b]	$\{110\}_{pc}$; $\beta > \pi/2$ $c_m > a_m/\sqrt{2}$ and $b_m/\sqrt{2}$	$a_{pc}^2 = b_{pc}^2 = (a_m/2)^2 + (b_m/2)^2$; $c_{pc} \approx c_m$	$c_{pc} > a_{pc} = b_{pc}$; a_{pc}, b_{pc} and c_{pc} all degenerated
M_B[b]	$\{110\}_{pc}$; $\beta > \pi/2$ $c_m < a_m/\sqrt{2}$ and $b_m/\sqrt{2}$	$a_{pc}^2 = b_{pc}^2 = (a_m/2)^2 + (b_m/2)^2$; $c_{pc} \approx c_m$	$c_{pc} < a_{pc} = b_{pc}$; a_{pc}, b_{pc} and c_{pc} all degenerated
M_C[c]	$\{100\}_{pc}$; $\beta > \pi/2$ $c_m > a_m$ and b_m	$a_{pc} \approx a_m$; $b_{pc} \approx b_m$; $c_{pc} \approx c_m$	$c_{pc} > a_{pc}$ and b_{pc}; both a_{pc} and c_{pc} degenerated but not b_{pc}
O[c]	$\{100\}_{pc}$; $\beta > \pi/2$ $c_m > a_m = b_m$	$a_{pc} \approx a_m$; $b_{pc} \approx b_m$; $c_{pc} \approx c_m$	$c_{pc} = a_{pc} > b_{pc}$; both a_{pc} and c_{pc} degenerated but not b_{pc}

[a] c_m and a_m are always bounded by the monoclinic angle β in the monoclinic (mirror) plane, where $\beta \neq \pi/2$.

[b] Both M_A and M_B phases are similar in nature in that the a_m and b_m axes are rotated 45° about the $[001]_{pc}$ direction and are bounded by the monoclinic angle, $\beta \neq \pi/2$. They are both characterized by $c_{pc} \approx c_m$ and $a_{pc}^2 = b_{pc}^2 = (a_m/2)^2 + (b_m/2)^2$ because a_m and b_m are bounded by $\pi/2$. They, however, differ in the spontaneous strain, leading to $c_m > a_m$ and b_m for the M_A phase but $c_m < a_m$ and b_m for the M_B phase.

[c] The orthorhombic (O) phase may be treated as a special case of the M_C, of which $c_m = a_m$ and the volume of an orthorhombic cell is approximately double that of a corresponding pseudocubic cell.

M_B phase, in which the peak at $2\theta \approx 44.83°$ is one of the degeneracy peaks of c_{pc} of the M_B phase while its a_{pc} and b_{pc} peaks may have emerged with the main R peak to form the broad convoluted peak at $2\theta \approx 44.65°$. Alternatively, it may arise from R_{NT}, as suggested by Wang [14, 15]. In other words, figure 3(d) can be assigned to the following possible phase combinations: (a) R (i.e., d_4 in figure 3(d)) + R_{NT} (i.e. $d_1 + d_3$ in figure 3(d)) or (b) R (i.e. d_4 in figure 3(d)) +M_B (i.e. $d_1 + d_3 + d_4$ in figure 3(d)), where R and R_{NT} denote the microscopic and nanotwin rhombohedral domains, respectively.

The following observations suggest that these diffraction peaks belong to that of the $(R + R_{NT})$ but not the $(R + M_B)$ phase. Should the phase present be the M_B phase, the question thus arises as to what phase the d_2, d_5, d_6 and d_7 peaks represent in the unpoled state—this could mean three phases coexist at the unpoled state at 105 °C. It should be noted that, other than the eutectoid point where three phases coexist, a maximum of two phases are present in a two-component system under the equilibrium system. It is thus less likely for the M_B phase to be present in a temperature range of 90–130 °C. Further evidence to support the $(R + R_{NT})$ comes from the observation that only a sharp current signal (figure 2(a)) and a single dielectric anomaly were detected in the temperature region of 90–110 °C. All these indicate that possibly only one phase transformation, i.e. that of R–T, is involved over the said temperature range. Based on the above results, we may conclude that the relevant diffraction peaks are those of the R_{NT}.

Meanwhile, in the poled sample, the d_7 and d_8 peaks (figure 4(d)) must also pertain to those of the R_{NT} domains. This is because, other than the anomaly corresponding to the R–T transformation which shows up in both the dielectric permittivity and thermal current density measurements, no other polarization activities could be detected from such measurements in the region of 80–115 °C.

4.2. Identification of tetragonal nanotwin diffractions

The present work shows that, at 115 °C for both the unpoled and poled samples, six diffraction peaks emerged (figures 3(e) and 4(d)). These diffraction peaks may be assigned as (a) M_B (i.e. d_1, d_3, d_4 and d_6) +T (i.e. d_2 and d_5), (b) M_C (i.e. d_1, d_2, d_3, d_4 and d_6) +T (i.e. d_2 and d_5) or (c) T_{NT} (i.e., d_1, d_3, d_4 and d_6) +T (i.e. d_2 and d_5).

We may rule out possibilities (a) and (b) as transformations of the type M_B–C and M_C–C are not permitted by the crystal transformation theory [12, 25]. The following reason also helps to rule out the presence of the M_C phase. That is, typically $a_{pc} \neq b_{pc}$ for the M_C phase. This means that the a_{pc} and b_{pc} diffractions for the M_C should not lie on the same Bragg angle and that the b_{pc} diffraction is non-degenerated. These features are not borne out by the diffraction shown in figures 3(e) and 4(d). Furthermore, figures 1 and 2 revealed only one anomaly in dielectric permittivity and one major thermal current signal in the range of 140–170 °C concerned. Based on these observations, we may rule out the existence of either the M_B or M_C phase and conclude that the relevant diffraction peaks are those of the T_{NT}.

It should be mentioned that, upon heating from 115 to 155 °C (figures 3(e) and (f) and 4(e) and (f)), the various diffraction peaks are of asymmetrical degeneracy. This is

especially pronounced for the poled sample. This observation may be understood from the strained state and the unbalanced population of R_{NT} and T_{NT} formed in the material near the T_{R-T}. Note that both the PZN–4.5%PT [17, 22] and PZN–7%PT single crystals undergo a similar phase transformation upon ZFH.

5. Conclusions

The present work shows that the room temperature state of both the unpoled and poled PZN–7%PT consists largely of microscopic R domains, although minor R_{NT} domains may be present. Through combined bulk property characterization (via dielectric permittivity and thermal current density measurements) and HR-XRD study, the phase transformation path of both the unpoled (annealed) and annealed-and-poled PZN–7%PT under ZFH conditions were identified as $R - (R + R_{NT} + T + T_{NT}) - (T + T_{NT}) - C$. The R_{NT} and T_{NT} domains occurred in the temperature vicinity of the R–T transformation, possibly as a means to alleviate the transformation stress in the material. Care must thus be exercised in interpretation of the HR-XRD spectra of bulk crystals as they can be easily be mistaken for those arising from the monoclinic state. Compared with the unpoled state, the HR-XRD patterns revealed that the poled crystal is in a strained state such that the HR-XRD spectra are distorted to various degrees.

Acknowledgments

The authors gratefully acknowledge the financial support from the Ministry of Education (Singapore) and National University of Singapore, via research grants nos. R-265-000-221-112, R-265-000-257-112, R-265-000-261-123/490 and R-265-000-257-731, support received by SSLS via NUS Core Support C-380-003-003-001, A*STAR/MOE RP 3979908M, A*STAR 012 105 0038, A*STAR R144-000-053-303, ARF R-144-000-53-107 and A*STAR 012 101 0131 grants, and from the National Science Council of Taiwan via grant no. 95-2112-M-030-001.

References

[1] Park S-E and Shrout T R 1997 *J. Appl. Phys.* **82** 1804–11
[2] Liu S-F, Park S-E, Shrout T R and Cross L E 1999 *J. Appl. Phys.* **85** 2810–4
[3] Fu H and Cohen R E 2000 *Nature* **403** 281–3
[4] Bellaiche L, Garcia A and Vanderbilt D 2000 *Phys. Rev. Lett.* **84** 5427–30
[5] Vanderbilt D and Cohen M H 2001 *Phys. Rev.* B **63** 094108
[6] Noheda B, Cox D E, Shirane G, Park S-E, Cross L E and Zhong Z 2001 *Phys. Rev. Lett.* **86** 3891–4
[7] Cox D E, Noheda B and Shirane G 2001 *Appl. Phys. Lett.* **79** 400–2
[8] Noheda B, Zhong Z, Cox D E, Shirane G, Park S-E and Rehrig P 2002 *Phys. Rev.* B **65** 224101
[9] La-Orauttapong D, Noheda B, Ye Z-G, Gehring P M, Toulouse J, Cox D E and Shirane G 2002 *Phys. Rev.* B **65** 144101
[10] Noheda B 2002 *Curr. Opin. Solid State Mater. Sci.* **6** 27–34
[11] Lu Y, Jeong D-Y, Cheng Z-Y, Shrout T and Zhang Q M 2002 *Appl. Phys. Lett.* **80** 1918–20
[12] Forrester J S, Plitz R O, Kisi E H and McIntyre G J 2001 *J. Phys.: Condens. Matter* **13** L825–33
[13] Kisi E H, Piltz R O, Forrester J S and Howard C J 2003 *J. Phys.: Condens. Matter* **15** 3631–40
[14] Wang Y U 2006 *Phys. Rev.* B **74** 104109
[15] Wang Y U 2007 *Phys. Rev.* B **76** 024108
[16] Wang H, Zhu J, Lu N, Bokov A A, Ye Z-G and Zhang X W 2006 *Appl. Phys. Lett.* **89** 042908
[17] Lim L C, Chang W S, Rajan K K, Shanthi M, Yang P, Moser H O, Tu C-S, Wang F-T, Tseng C-T, Bhalla A S and Guo R 2008 *J. Appl. Phys.* **103** 084122
[18] Uesu Y, Matsuda M, Yamada Y, Fujishiro K, Cox D E, Noheda B and Shirane G 2002 *J. Phys. Soc. Japan* **71** 960–5
[19] Lim L C and Rajan K K 2004 *J. Cryst. Growth* **271** 435–44
[20] Chang W S, Shanthi M, Rajan K K, Lim L C, Wang F T, Tseng C T, Tu C S, Yang P and Moser H O 2007 *J. Appl. Phys.* **101** 124104
[21] Chang W S, Lim L C, Wang F-T, Tu C-S and Yang P 2008 *J. Appl. Phys.* **103** 074110
[22] Chang W S, Lim L C, Yang P, Tu C-S, Wang F-T and Tseng C-T 2008 *J. Appl. Phys.* **104** 054102
[23] Blinc R, Laguta V V, Zalar B and Banys J 2006 *J. Mater. Sci.* **41** 27–30
[24] Liu T and Lynch C S 2006 *Contin. Mech. Thermodyn.* **18** 119–35
[25] Sergienko I A, Gufan Y M and Urazhdin S 2002 *Phys. Rev.* B **65** 144104